molecular pharmaceutics

pubs.acs.org/molecularpharmaceutics

Article

Head-to-Head Comparison of the *in Vivo* Performance of Highly Reactive and Polar ^{18}F-Labeled Tetrazines

Lars Hvass,*[,‖] Marius Müller,[‖] Markus Staudt, Rocio García-Vázquez, Tobias K. Gustavsson, Vladimir Shalgunov, Jesper T. Jørgensen, Umberto M. Battisti,* Matthias M. Herth,* and Andreas Kjaer*

Cite This: *Mol. Pharmaceutics* 2025, 22, 1911−1919

Read Online

ACCESS | Metrics & More | Article Recommendations | Supporting Information

ABSTRACT: Pretargeted imaging harnessing tetrazine ligation has gained increased interest over recent years. Targeting vectors with slow pharmacokinetics may be visualized using short-lived radionuclides, such as fluorine-18 (^{18}F) for positron emission tomography (PET), and result in improved target-to-background ratios compared to conventionally radiolabeled slowly accumulating vectors. We recently developed different radiochemical protocols enabling the direct radiofluorination of various tetrazine scaffolds, resulting in the development of various highly reactive and polar ^{18}F-labeled tetrazines as lead candidates for pretargeted imaging. Here, we performed a direct head-to-head-comparison of our lead candidates to evaluate the most promising for future clinical translation. For that, all ^{18}F-labeled tetrazine-scaffolds were synthesized in similar molar activity for improved comparability of their *in vivo* pretargeting performance. Intriguingly, previously reported dicarboxylic acid lead candidates with a net charge of −1 were outperformed by respective monocarboxylic acid derivatives bearing a net charge of 0, warranting further evaluation of such scaffolds prior to their clinical translation.

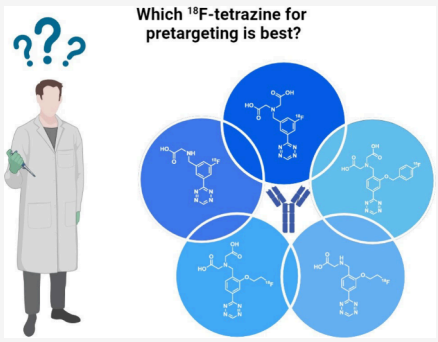

KEYWORDS: *pretargeting, bioorthogonal chemistry, tetrazine ligation, fluorine-18, phenyl-tetrazines*

INTRODUCTION

Pretargeted imaging has become an appealing technique in positron emission tomography (PET).[1−3] Pretargeting involves using macromolecules, typically antibodies (Abs), combined with small molecular probes to improve imaging contrast and reduce patient radiation exposure.[1−3] This is achieved by administering a tagged nonradioactive Ab several days before injecting the radioactive imaging agent. The radioactive agent can then react specifically with the tag of Ab *in vivo*, creating a radiolabeled Ab for targeted imaging. This strategy is often used for cancer diagnostics, but new data has also shown its potential for applications in the central nervous system (CNS).[4−7] To function within a living organism, pretargeting exploits a specific type of reaction. These reactions, based on their properties, are referred to as bioorthogonal.[8,9] Among bioorthogonal reactions, the tetrazine ligation between a *trans*-cyclooctene (TCO) and a tetrazine (Tz) has stood out as the most promising due to its high selectivity and rapid reaction kinetics.[1,10−12] The tetrazine ligation involves an inverse-electron-demand Diels−Alder (IEDDA) reaction followed by a retro-Diels−Alder reaction, resulting in the formation of nitrogen gas (Figure 1A).[13] This irreversible reaction yields a chemically stable dihydropyridazine.[13] Typically, due to their properties, TCOs are conjugated to the pretargeting vector, such as Abs, while tetrazines are used as radionuclide carrier.[12] On the other hand, a few examples have been reported where the TCOs were used as radionuclide carrier.[14−16]

The first and pioneering Tzs developed for this purpose contained chelators such as NOTA and DOTA and were thus labeled with radiometals.[17−20] Recently, new methods have been reported for labeling highly reactive Tzs with various covalently bound nuclides.[21−26] Notably, fluorine-18 (^{18}F) has been extensively explored by different research groups for labeling of several tetrazine scaffolds due to its ideal imaging properties.[27−33] In recent years, our team has developed a few new methodologies for labeling of highly reactive tetrazines with ^{18}F.[34−39] This work culminated with the development of several small molecular probes based on ^{18}F-labeled tetrazines (Figure 1B, compounds **1**−**5**).[34−39] Compounds [^{18}F]**1** and [^{18}F]**3** were previously published by us.[35,39] Probes [^{18}F]**2** and [^{18}F]**4** are structurally related to **1** and **3** but have a different overall charge (net charge is 0 vs −1). Finally compound [^{18}F]**5** was designed as a hybrid between compounds **1** and **3**. All these molecules displayed favorable pharmacokinetics *in vivo* with tumor accumulation and a high tumor-to-muscle ratio. In this article, we conducted a head-to-head study to compare *in vivo* performance of our leading ^{18}F-tetrazines. All molecules

Received: October 3, 2024
Revised: January 27, 2025
Accepted: January 28, 2025
Published: March 13, 2025

https://doi.org/10.1021/acs.molpharmaceut.4c01129
Mol. Pharmaceutics 2025, 22, 1911−1919

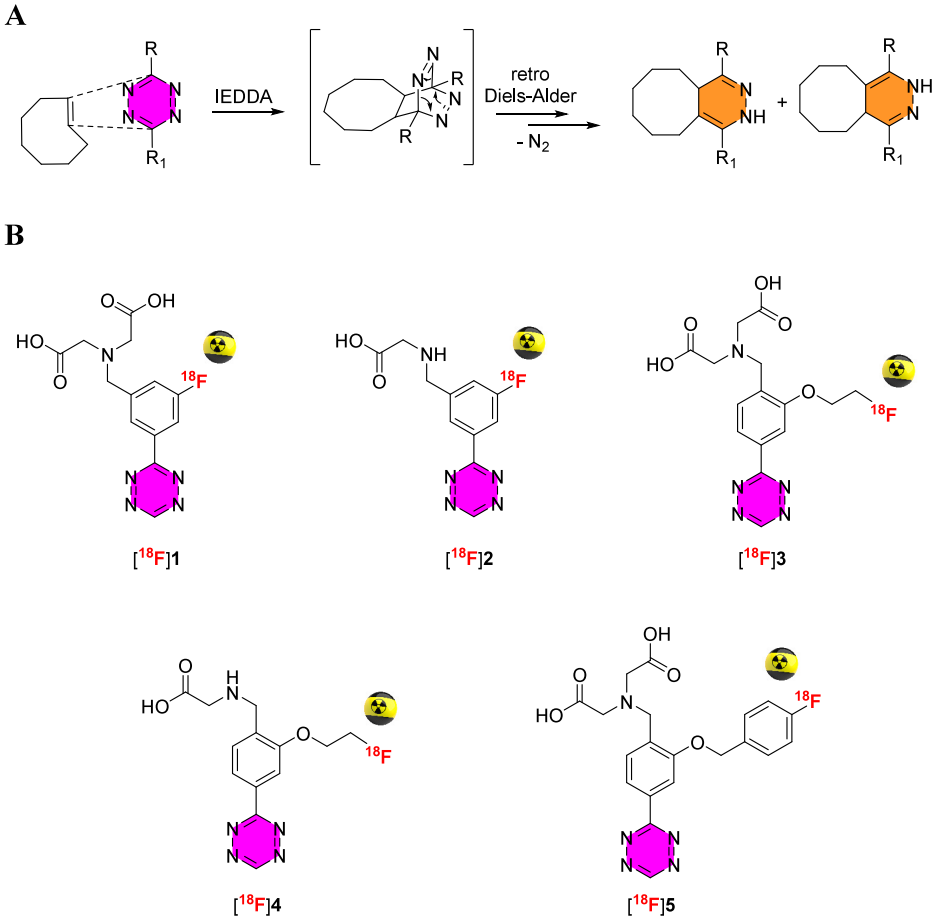

Figure 1. (A) The tetrazine−TCO ligation. (B) Chemical structures of the ^{18}F-tetrazines evaluated in this study.

were tested in TCO−CC49 antibody-pretreated xenograft mice with TAG72 overexpressing tumor cells LS174T. This study is based on the relationship between structure and pharmacokinetics and will assist us in selecting the most promising ^{18}F-labeled tetrazine and in translating its synthesis and use in the clinic.

MATERIALS AND METHODS

Radiochemistry: General Information. [^{18}F]Fluoride was produced via the (p,n)-reaction in a cyclotron (60 mikroA CTI Siemens or 40 mikroA Scanditronix) by irradiating [^{18}O]H_2O with an 11 MeV (CTI siemens) or 16 MeV (Scanditronix) proton beam. Analytical HPLC was performed on a Dionex system connected to a P680A pump, a UVD 170U detector, and a Scansys radiodetector. The system was controlled by Chromeleon software. Analytical HPLC method: Thermo Fisher Ultimate with a C-18 column (Luna 5 μm C18(2) 100 Å, 150 mm × 4.6 mm and Luna 5 μm PFP(2) 90 Å 150 mm × 4.6 mm). Eluents: A, H_2O with 0.1% TFA; B, MeCN with 0.1% TFA. Gradient from 100% A to 100% B over 12 min, back to 100% A over 3 min, flow rate 2 mL/min. Detection was by UV absorption at δ = 254 nm on a UVD 170 U detector.

Radiochemical conversion (RCC) of all radiolabeled compounds was determined by analyzing an aliquot of the reaction mixture by radio-HPLC and obtained by integrating the radioactive peaks from the reaction solution. The products were characterized by comparing the radio-HPLC trace of the reaction mixture to the HPLC UV traces of the authentic ^{19}F-reference samples, respectively.

The identity of [^{18}F]**1**−**5** was determined by comparing the retention time of the product's radio-HPLC trace with the HPLC-UV trace of the respective ^{19}F-references **1**−**5**. The decay-corrected radiochemical yield (RCY) was determined comparing the activity of dry [^{18}F]TBAF and that of the product after semipreparative HPLC purification. The activity of the HPLC-purified product was decay corrected to the time the activity of the dry [^{18}F]TBAF being measured. The molar activity (A_m) of [^{18}F]**1**−**5** was determined by integrating the area of the UV absorbance peak corresponding to the radiolabeled product on the HPLC chromatogram. This area was compared to a standard row of UV peak integrals corresponding to different injected concentrations of **1**−**5** (triplicate for each concentration) at the same injection volume, allowing the calculation of the total concentration (in μg/mL or nmol/mL) of Carrier-Tz in the formulated solution. The activity of the HPLC sample of [^{18}F]**1**−**5**, its total volume, as well as the concentration of the Carrier-Tz, allowed the calculation of the A_m.

The radiochemical purity (RCP) of the formulated product solution was assessed by integrating the area of the formulated product radio-HPLC trace and comparing its integral to that of any other radioactive byproducts.

Preparation of Anhydrous [^{18}F]F Fluoride for Radiolabeling. QMA anion exchange cartridge (Sep-Pak Accel Plus QMA Plus Light, bicarbonate form, Waters) was washed with EtOH (10 mL), 0.5 M K_3PO_4 (10 mL), and H_2O (10 mL),

https://doi.org/10.1021/acs.molpharmaceut.4c01129
Mol. Pharmaceutics 2025, 22, 1911−1919

and dried with air (10 mL) before use. Irradiated $[^{18}O]H_2O$ containing $[^{18}F]F^-$ was passed through a preconditioned QMA anion exchange cartridge. $[^{18}F]F^-$ trapped on the QMA anion exchange cartridge was then eluted with a mixture of a 20 nM tetrabutyl ammonium salt (for $[^{18}F]$**1**, $[^{18}F]$**2**, and $[^{18}F]$**4**: Bu_4NOTf; for $[^{18}F]$**3**: Bu_4NOMs) in MeOH (1 mL) into a septum-capped 4 mL glass vial. The resulting mixture was then concentrated to dryness at 100 °C under a continuous stream of nitrogen (N_2) for 15 min to give $[^{18}F]Bu_4NF$ as a colorless oil.

General Procedure for the Automated Synthesis of [^{18}F]1, [^{18}F]2, and [^{18}F]5. Automated synthesis was performed on a Scansys Laboratorieteknik synthesis module. A solution of either **1a** (10 μmol) and $Cu(OTf)_2(Py)_4$ (15 μmol, 10.2 mg) in dry DMA (1 mL), **2a** (10 μmol) and $Cu(OTf)_2(Py)_4$ (15 μmol, 10.2 mg) in dry DMA (1 mL), or **5a** (10 μmol) and $Cu(OTf)_2(Py)_4$ (15 μmol, 10.2 mg) in dry DMA (1 mL) was added to the reaction vial containing the dried $[^{18}F]Bu_4NF$ (15−17 GBq). The reaction mixture was left at 100 °C for 5 min. After cooling the mixture for 2.5 min down to approximately 55 °C, it was quenched with 2.2 mL of H_2O + 0.1% TFA. The crude reaction mixture was then passed through a Sep-Pak C18 Plus cartridge previously precondition with 10 mL of EtOH, 10 mL H_2O, and 10 mL of air. The Sep-Pak C18 Plus cartridge was then washed with H_2O (7 mL) and dried with air, followed by its elution with MeCN (3 mL) in a septum-capped 7 mL vial filled with TFA (1 mL). The solution was heated to 80 °C for 5 min, followed by its concentration under a gentle nitrogen flow at 85 °C for approximately 15 min (concentration down to 50−100 μL) and addition of 2.2 mL of H_2O + 0.1% TFA. The resolubilized solution was then purified via semipreparative HPLC-purification (Thermo Fisher UltiMate 3000) with a Luna 5 μm C-18(2) column (100 Å, 250 mm × 10 mm) using an isocratic method based on 15% EtOH/H_2O + 0.1% TFA and a flow rate of 3.2 mL/min (for $[^{18}F]$**1** and $[^{18}F]$**3**) or an isocratic method based on 40% MeCN/H_2O + 0.1% TFA and flow rate f 4 mL/min (for $[^{18}F]$**5**). The product fraction was collected in a 10 mL glass vial filled with 1 mL of sterile 0.1 M phosphate buffer (pH 7.4). The isolated products collected from the HPLC, approximately 2.3 GBq for $[^{18}F]$**1** and approximately 1 GBq for $[^{18}F]$**2**, and approximately was then formulated by the dilution with PBS (pH = 7.4), adjusting the EtOH concentration to below 5% and the final activity concentration to approximately 100 MBq/mL. The automated synthesis including purification and concentration of the $[^{18}F]F^-$, copper-mediated radiofluorination, Sep-Pak C18 Plus cartridge purification, deprotection, semipreparative-HPLC purification, and formulation was performed within 90 min.

Formulation of $[^{18}F]$**5** was performed differently. The isolated product collected from HPLC (approximately 0.14 GBq for $[^{18}F]$**5**) was then diluted in 50 mL of H_2O + 0.1% TFA and passed through a Sep-Pak Light C18 cartridge, which was previously preconditioned with EtOH (10 mL), H_2O (10 mL), and dried with air (10 mL). After the whole product solution had passed through the Sep-Pak Light C18 cartridge, $[^{18}F]$**5** was eluted with EtOH (1 mL), dried at 50 °C under a continuous stream of nitrogen for 11 min, and formulated with 0.1 M phosphate buffer (pH 7.4) with a final activity concentration of 76 MBq/mL and an EtOH concentration <5%. The automated synthesis including purification and concentration of $[^{18}F]$TBAF, labeling, HPLC separation, and formulation was performed over the course of 100 min.

General Procedure for the Automated Synthesis of [^{18}F]3 and [^{18}F]4. Automated synthesis was performed on a Scansys Laboratorieteknik synthesis module. A solution of either **7** (6.2 μmol) or **8** (6.2 μmol) in tBuOH/DMSO (5/1; 1 mL) was added to the reaction vial containing the dried $[^{18}F]Bu_4NF$ (15−17 GBq). The reaction was left at 100 °C for 5 min. After cooling the reaction mixture for 2.5 min down to approximately 55 °C, it was quenched with 2.2 mL of H_2O + 0.1% TFA. The crude reaction mixture was then passed through a Sep-Pak C18 Plus cartridge previously precondition with 10 mL of EtOH, 10 mL of H_2O, and 10 mL of air. The Sep-Pak C18 Plus cartridge was then washed with H_2O (7 mL) and dried with air, followed by its elution with MeCN (3 mL) into a septum-capped 7 mL vial filled with TFA (1 mL). The solution was heated to 80 °C for 5 min, followed by its concentration under a gentle nitrogen flow at 85 °C for approximately 15 min (concentration down to 50−100 μL) and addition of 2.2 mL of H_2O + 0.1% TFA. The resolubilized solution was then purified via semipreparative HPLC-purification (Thermo Fisher UltiMate 3000) with a Luna 5 μm C-18(2) column (100 Å, 250 mm × 10 mm) using an isocratic method based on either 15% EtOH/H_2O 0.1% TFA for $[^{18}F]$**3** or 10% EtOH/H_2O + 0.1% TFA for $[^{18}F]$**4** and a flow rate of 4 mL/min ($[^{18}F]$**3**) or 3.2 mL/min ($[^{18}F]$**4**). The product fraction was collected into a 10 mL glass vial filled with 1 mL of sterile 0.1 M phosphate buffer (pH 7.4). The isolated products collected from the HPLC, approximately 0.4 GBq for both $[^{18}F]$**3** and $[^{18}F]$**4**, was then formulated by dissolving the collected fraction in H_2O (50 mL) and passing the solution through a Sep-Pak C18 Light cartridge previously preconditioned with 10 mL of EtOH, 10 mL of H_2O, and 10 mL of air. The trapped $[^{18}F]$**3** and $[^{18}F]$**4** was then eluted with EtOH (1 mL) and concentrated at 50 °C under a continuous stream of nitrogen for approximately 10 min, followed by the resolubilization in sterile 0.1 M PBS (pH 7.4) with a final activity concentration of 57 MBq/mL ($[^{18}F]$**3**) or 100 MBq/mL ($[^{18}F]$**4**) and an EtOH concentration <5%. The automated synthesis including purification and concentration of $[^{18}F]$TBAF, labeling, HPLC separation, and formulation was performed over the course of 100 min.

Tz Core Reactivity Test. The reaction between $[^{18}F]$**1**−**5** and TCO-PNB was performed by mixing the formulated radiolabeled tetrazine (100 μL) with 5 μL of the commercially available TCO-PNB ester dissolved in DMF (2 mg/mL) in an analytical HPLC vial. The solution was gently shaken and left for 1 min before it was injected on analytical HPLC for analysis. The reaction was monitored by TLC and HPLC.

Antibody TCO Functionalization and ELISA. CC49 antibody was functionalized with TCO and the TCO load quantified as described in the Supporting Information (SI). The antigen-binding affinity of TCO-modified CC49 was determined using an indirect ELISA assay. A 96-well plate (Corning) was coated with 1 μg/mL mucin type I−S (Sigma-Aldrich, M3895) in PBS and incubated at +4 °C overnight. Next, blocking was performed with ELISA blocking buffer (PBS, 1% BSA) for 2 h at room temperature. A 50 nM serial dilution of TCO−CC49 and unmodified CC49 was incubated in ELISA buffer (PBS, 0.1% BSA, 0.05% Tween-20) for 2 h at room temperature. Subsequently, peroxidase-conjugated rabbit antimouse IgG secondary antibody (1:2000, Thermofisher, A16160) was added and incubated at room temperature for 1 h. ELISA was developed with TMB solution (Thermofisher, 34028), stopped with 2 M HCl, and read at 450 nm

https://doi.org/10.1021/acs.molpharmaceut.4c01129
Mol. Pharmaceutics 2025, 22, 1911−1919

Table 1. Structural Scaffolds, Molecular Weight, clogD$_{7.4}$, Labelling Method, Radiochemical Yield, and Net Charge of All Investigated Tetrazine Derivatives

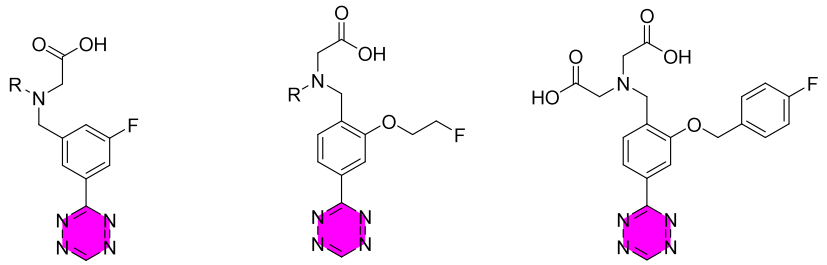

A B 5

tetrazine[a]	MW[b]	scaffold	R_1	ClogD$_{7.4}$[c]	labeling method	RCY[f]	net charge
1[a]	321.1	A	$-CH_2COOH$	−6.93	CMRF[d]	19.9	−1
2[a]	263.1	A	−H	−2.89	CMRF[d]	8.4	0
3[a]	365.1	B	$-CH_2COOH$	−6.97	SN_2[e]	3.4	−1
4[a]	307.1	B	−H	−3.03	SN_2[e]	5.1	0
5[a]	427.1			−5.45	CMRF[d]	1.2	−1

[a]Notes: The compounds were obtained as trifluoroacetate salt. [b]Molecular weight (MW) of the selected compounds. [c]Calculated distribution coefficient at physiological pH (7.4) in Chemicalize software. [d]Copper-mediated radiofluorination. [e]Bimolecular nucleophilic substitution. [f]Radiochemical yield.

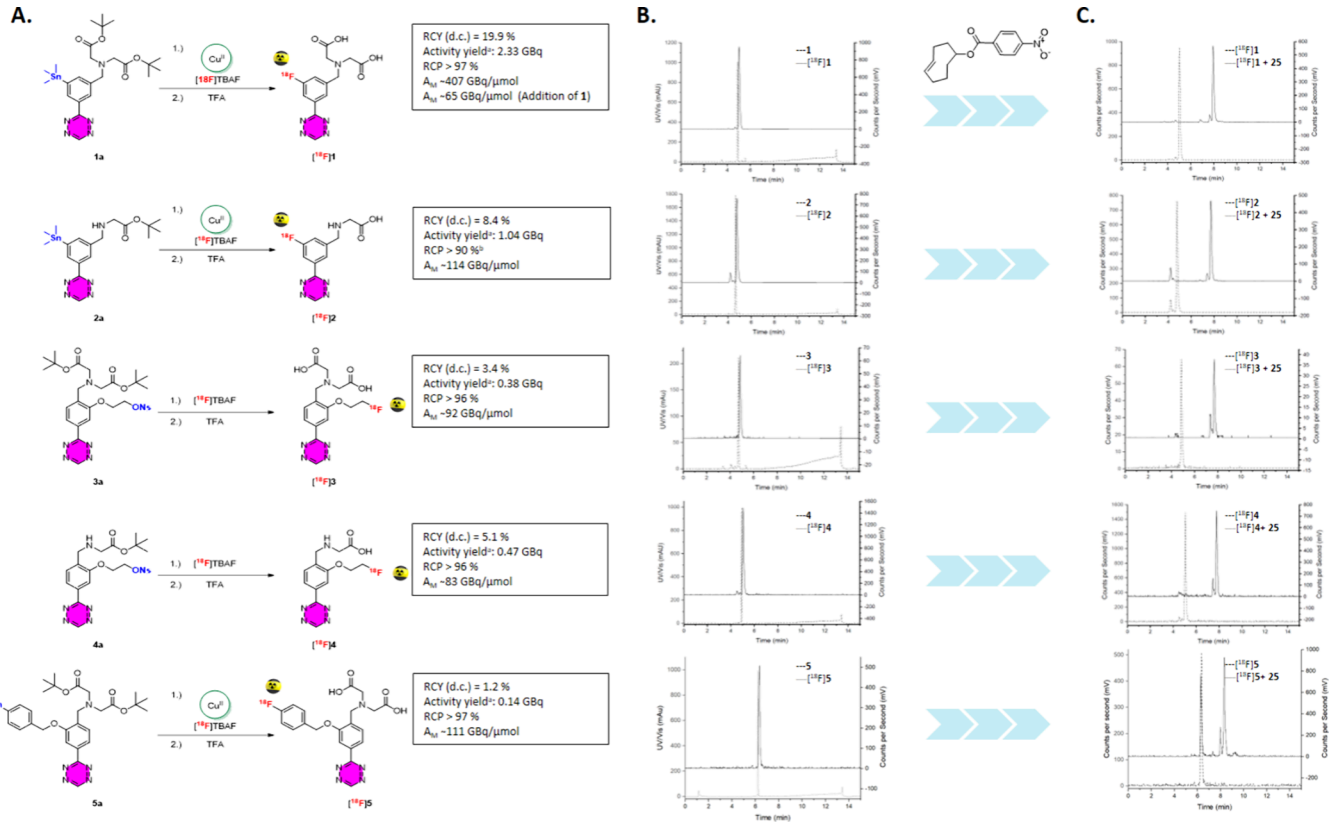

Figure 2. Radiosynthesis of [^{18}F]**1**−**5** prior to their injection into LS174T xenograft nude mice. (A) Radiosynthesis of [^{18}F]**1**−**5**. (B) Analytical HPLC of reference compounds **1**−**5** (UV/vis 254 nm; R_t = **1**, 4.910 min; **2**, 4.650 min; **3**, 4.720 min; **4**, 4.927; **5**: 6.223 min) (dashed graphs) and radio-HPLC of the formulated [^{18}F]**1**−**5** (R_t(RCP) = [^{18}F]**1**, 5.020 min (>97%); [^{18}F]**2**, 4.767 min (>90%[a]); [^{18}F]**3**, 4.853 min (>96%); [^{18}F]**4**, 5.057 min (>96%); [^{18}F]**5**, 6.337 min (>97%)) (black graphs). (C) Radio-HPLC of the formulated [^{18}F]**1**−**5** before (dashed graph) and after (black graph) the addition of TCO-PNB ester (performed 20−30 min after formulation). [a]RCP of [^{18}F]**2** lower than observed for previous syntheses and purifications. HPLC conditions: Luna 5 µm C18(2) 100 Å, 150 mm × 4.6 mm eluted with a gradient of ACN with 0.1% v/v TFA (solvent B) in water with 0.1% v/v TFA (solvent B) at 2 mL/min. Gradient: 0−1 min, 0% B; 1−11 min, 0−100% B; 11−12 min, 100% B; 12−13 min, 100−0% B; 13−15 min, 0% B.

Cell Culture. LS174T (ATCC, USA) TAG72-expressing human colorectal adenocarcinoma cells were grown in Eagle's Minimum Essential Medium (signa-Aldrich) supplemented with 10% fetal bovine serum, 1% penicillin/streptomycin,

https://doi.org/10.1021/acs.molpharmaceut.4c01129
Mol. Pharmaceutics 2025, 22, 1911−1919

nonessential amino acids, and sodium pyruvate. Media was replaced regularly, and cells were incubated in a water vapor saturated 5% CO_2 atmosphere at 37 °C. Cells were authenticated by short tandem repeat analysis (ATCC).

In Vivo Evaluation. All animal studies are approved by the Danish Animal Experimentation Council (2021-15-0201-01041) and carried out in compliance with EU directive 2010/63/EU of the EU legislation on the protection of animals used for scientific purposes. Five-week-old Balb/cAnN-Foxn1$^{nu/nu}$Rj mice acquired from Janvier were housed at the University of Copenhagen. Here, animals were kept in a 12:12 light/dark cycle and fed chow *ad libitum*. After a one-week acclimatization period, 5 million LS174T cells were injected subcutaneously on the left flank under general anesthesia in 100 μL of PBS. Approximately 10 days after inoculation, mice were included in experiments. In a pilot experiment a suitable antibody dose was determined by injecting 1.5, 3, 6.25, 12.5, 25, 50, or 100 μg (n = 3, each group) CC49-TCO in the lateral tail vein 3 days prior to injection with [^{111}In]DOTA-PEG11-Tz ([^{111}In]DOTA-tz) (SI, Figure S22). Two hours later, mice were euthanized, tumors, blood, spleen, kidney, muscle, heart, liver, and lung tissue were resected and weighed, and activity content was determined using an automated gamma counter (Hidex, Finland). Activity was determined as %ID/g.

For the comparison experiment, mice were randomized to experimental groups and injected in the lateral tail vein with 50 μg of either CC49-TCO, or unmodified CC49 in 100 μL of PBS. n = 4 for each group and each compound, except for [^{18}F]**3**, for which n = 3 for CC49-TCO and n = 2 for CC49. Three days later, mice were injected with 4−9 MBq [^{18}F]**1**−**5** intravenously in 100 μL of PBS solution. Injection activities were corrected for waste post injection. 1, 2, and 3 h after injection, mice were PET/CT scanned (Inveon, Siemens Medical Solutions, USA). During scans, mice were anesthetized by breathing 30% oxygen enriched air containing 3.5−4.0% sevoflourane. CT scan parameters were: 360 projections, tube voltage 65 kV, and exposure time 440 ms, reconstructed with 2× downsampling. PET parameters: timing window 3.438 ns, and energy window 350−650 keV. Four mice were scanned simultaneously and body temperature kept constant by means of a water heated bed system modified from.[40] PET sinograms were reconstructed using an OSEM3D/SP-MAP algorithm with scatter and attenuation correction in the Inveon Acquisition Workplace (Siemens Medical Solutions, USA). Regions of interest (ROI) were manually drawn on the tumor, heart ventricle, and muscle. For the abdomen, as CT scans do not provide adequate soft tissue contrast to delineate abdominal organ segments such as small intestine, cecum, and colon, a spherical ROI was placed in the ventral abdominal region, taking care not to include signal from the bladder or kidney. Activity concentration was then expressed as %ID/g. After final PET/CT scan, two mice from each group were transcardially perfused with saline (flow 5 mL/min) prior to resection of tumor, spleen, kidney, muscle, heart, liver, and lung tissue, as to indicate signal contribution from radiolabeled antibody in the blood. Resected tissues were weighed and activity content determined using an automated gamma-counter using a 20% energy window around 511 keV,and activity concentration expressed as %ID/g.

RESULTS AND DISCUSSION

Synthesis and Characterization. Compounds **1**−**4** and precursors **1a** and **3a** were synthesized as previously described.[35,39] The synthesis of compound **5** and precursors **2a**, **4a**, and **5a** is described in detail in the Supporting Information. All molecules, including their intermediates, were analyzed and characterized via ^{1}H NMR, ^{13}C NMR (Supporting Information). Once the precursors were synthesized, the tetrazine constructs were then radiolabeled using different methodologies (Table 1, Figure 2).

Radiochemistry. [^{18}F]**1** and [^{18}F]**3** were synthesized as previously described.[35,37,39] Similar to [^{18}F]**1**, [^{18}F]**2** and [^{18}F]**5** were obtained via copper-mediated radiofluorination and subsequent Boc- and *tert*-butyl ester deprotection in a nonoptimized decay-corrected radiochemical yield (RCY) of 9.2 ± 1.1% ([^{18}F]**2**, n = 3) and 1.5 ± 0.6% ([^{18}F]**5**, n = 3) after semipreparative-HPLC purification. In contrast, precursor **4a** was subjected to aliphatic radiofluorination conditions as previously reported by Battisti et al. for the radiosynthesis of [^{18}F]**3**.[35] Unexpectedly, yellow discoloration of the reaction mixture was observed. Subsequent deprotection and semipreparative HPLC-purification did not yield the desired product [^{18}F]**4**. We hypothesized that the displacement of PO_4^{3-} ions, used for the preconditioning, during the elution of [^{18}F]F$^-$ from the quaternary methylammonium (QMA) anion exchange cartridge resulted in a too basic reaction mixture, leading to the degradation of the Tz core of **4a**. Indeed, adjusting the preconditioning anion of the quaternary ammonium exchange cartridge from the previously reported PO_4^{3-} to the nonbasic Cl$^-$ yielded [^{18}F]**4** in a not further optimized RCY of 4.5 ± 1.0% (n = 3) after semipreparative HPLC-purification. All radiofluorinated Tzs were reacted with TCO-PNB to check the integrity of the tetrazine core. All molecules showed full click with the formation of new peaks at different retention times (Figure 2).

***In Vivo* Pretargeting.** Subsequently, we compared [^{18}F]**1**−**5** for pretargeted imaging in CC49-TCO-pretreated mice bearing LS174T xenografts, a TAG72-expressing human colorectal adenocarcinoma. This specific cancer was selected as TAG-72 is a target known to induce cell internalization only to a small extend.[41] CC49 was loaded with 7.3 TCO/mAb as described in the experimental section, and 50 μg were injected intravenously. A previous study in the same tumor model found a dose of 50 μg of CC49-TCO to be an optimal trade-off between tumor %ID/g and tumor-to-organ ratios (SI, Figure S22). TCO modification only slightly reduced the binding affinity from 0.5 to 0.74 nM (SI, Figure S21). Three days after CC49-TCO injection, 4−9 MBq of each ^{18}F-labeled tracer was injected at high molar activity (Figure 2), and PET/CT scans acquired 1, 2, and 3 h after injection (Figure 3). Generally, only minute tumor accumulation (<0.1% ID/g) and low blood concentration (<0.13% ID/g) was evident for all groups previously administered with unmodified CC49 3 h after injection, (SI, Figure S23). Contrary, for mice pretreated with TCO-modified CC49, tumor accumulation increased over the investigated course of 3 h after injection of [^{18}F]**1**−**5** (Figure 3), whereas activity in blood remained close to initial levels (SI, Figure S23). This indicates that tetrazine was retained in the blood by circulating CC49-TCO antibody, and thus tumor to blood contrast may be further improved by the use of clearing agent or extracorporeal trapping step.[42,43] The lowest tumor uptake was evident for charged [^{18}F]**1** (0.66%ID/g). This value was marginally lower than what we previously observed[39] and can be related to several parameters. Of note, molar activity of the radiolabeled tetrazine and TCO load of CC49 as well as location of the nonselectively attached TCO residues to

https://doi.org/10.1021/acs.molpharmaceut.4c01129
Mol. Pharmaceutics 2025, 22, 1911−1919

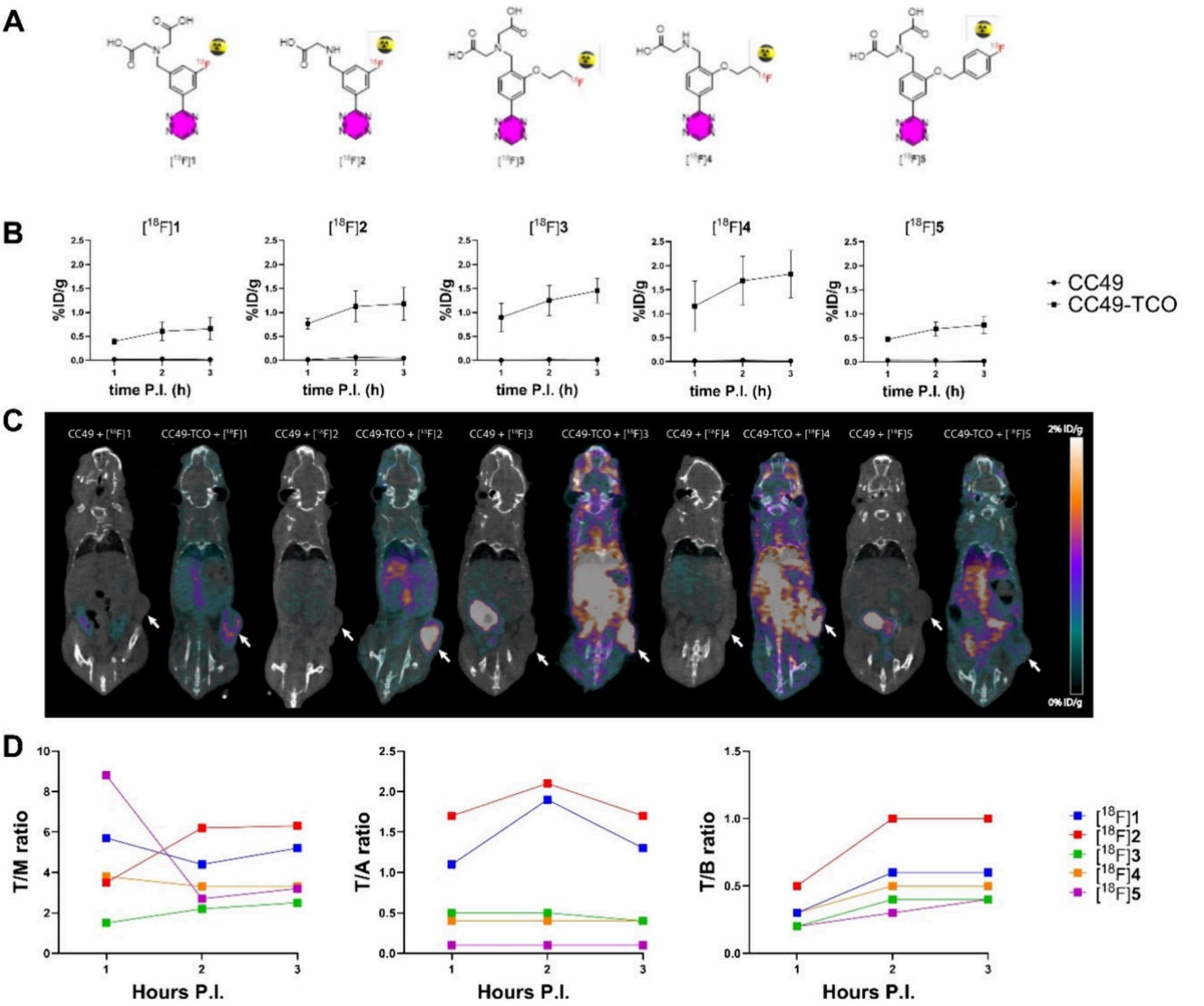

Figure 3. PET/CT scan of CC49-TCO pretargeted [^{18}F]**1**−**5** in nude mice bearing LS174T xenografts. (A) Structures investigated. (B) PET-image derived mean tumor uptake in CC49 and CC49-TCO pretargeted. (C) Representative PET images 3 h after injection. Arrows indicate tumors. (D) Tumor-to-muscle (T/M), tumor-to-abdomen (T/A), and tumor-to-blood (T/B) ratios.

the antibody, may affect tumor targeting and off-target accumulation.[44] Furthermore, age as well as body size of mice, altering the distribution volume, may give rise to discrepancies. However, due to the comparative nature of this study, we aimed to keep the molar activity of injected tetrazine similar and used the same production of TCO-modified CC49 antibody for all these compounds and to perform the studies closely spaced in time, avoiding trans−cis isomerization of TCO. As such, previously reported higher tumor accumulation of [^{18}F]**1**, indicates possible points of optimization, but does not discourage comparative investigation here.

Compound [^{18}F]**4** showed the highest peak tumor uptake of 1.8%ID/g 3 h after administration. Despite lower tumor uptake, [^{18}F]**2** demonstrates higher tumor-to-muscle and tumor-to-blood contrast (Figure 3) and 1.2%ID/g in tumor 3 h after injection. Even though [^{18}F]**3** shows similar tumor accumulation (1.5% ID/g), it is hampered by high muscle and blood retention as well as abdominal background, resulting in poor tumor-to-muscle (2.5), tumor-to-abdomen (0.4), and tumor-to-blood (0.4) ratios 3 h after administration (Figure 3). [^{18}F]**1** and [^{18}F]**5** demonstrated poor tumor accumulation of 0.66% ID/g and 0.77% ID/g, respectively. Thus, [^{18}F]**2** and [^{18}F]**4** appear to outperform their corresponding dicarboxylic acid derivatives ([^{18}F]**1** and [^{18}F]**3**, respectively) by virtue of peak tumor uptake in the case of [^{18}F]**4** but higher tumor-to-background ratio for [^{18}F]**2**.

Compounds [^{18}F]**1**−**5** mainly differ in polarity, net charge, and scaffold. Previous studies by Meyer and colleagues on tetrazine scaffolds modified with a linker and chelator for radiometal complexing found that generally, tracers with neutral net charge appeared to circulate for longer and clear the blood by liver and intestine.[20] While we do note a slight tendency toward increased abdominal residence of [^{18}F]**2** and [^{18}F]**4** relative to their less lipophilic and negatively charged counterparts ([^{18}F]**1** and [^{18}F]**3**) in both pretargeted and control animals, tetrazine scaffold appears to be dictating abdominal retention, which is not mediated by CC49-TCO. As such [^{18}F]**1** and [^{18}F]**2** demonstrated low abdominal retention (0.2 and 0.6%ID/g), and surprisingly, [^{18}F]**3** and [^{18}F]**4** higher (3.2 and 4.3%ID/g), and [^{18}F]**5** highest retention of 8.2%ID/g (Figure 3D, and SI, Figure S23D). Contrarily, we found that for all compounds kidney retention was ∼1%ID/g or less at *ex*

https://doi.org/10.1021/acs.molpharmaceut.4c01129
Mol. Pharmaceutics 2025, 22, 1911−1919

vivo biodistribution after final scan acquisition (SI, Figure S24), whereas, as mentioned above, blood retention was mediated by CC49-TCO (SI, Figure S23). This is expected due to the small and highly polar nature of the compounds, aimed at fast renal clearance. These findings suggest that a net charge of 0 might be ideal to achieve higher tumor accumulation, while scaffold A seems to have a more favorable clearance regardless of net charge. Balancing these factors are important to achieving favorable pharmacokinetics for diagnostic purposes. Accordingly, tumor accumulation should be rapid and clearance fast to allow for adequate tumor-to-background contrast in combination with short-lived radionuclides, which also allows for early imaging time points and lower dosimetry burden to the patient.

To assess the impact of circulating *in vivo* radiolabeled antibody on tumor activity levels, we transcardially perfused half of the scanned animals immediately after the final scan. Perfusion with saline prior to *ex vivo* biodistribution revealed unchanged tumor accumulation after blood was rid from the tissue, indicating low signal contribution from circulating antibody in tumors (Figure 4), whereas for other organs, there was a tendency of washout in lung and liver (SI, Figure S24.

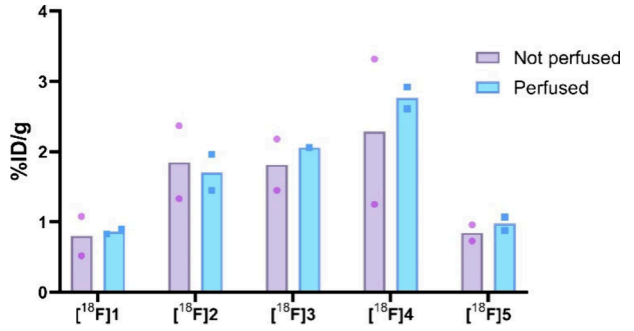

Figure 4. *Ex vivo* tumor biodistribution conducted after final scan (3 h after injection). For each compound, scanned animals were either dissected immediately or perfused with saline prior to dissection.

A limitation of this study is the lack of detailed biodistribution data for abdominal organs. Future studies will aim at detailing these factors further, as well as identify optimal dose regime for [^{18}F]**2** and [^{18}F]**4** relative to antibody dose.

CONCLUSIONS

Radiosynthesis of [^{18}F]**1**−**5** proceeded via previously reported nucleophilic substitutions or copper-mediated radiofluorinations. [^{18}F]**1**−**5** were obtained in low to moderate yield and similar molar activities ranging between 65−114 GBq/μmol. Compound [^{18}F]**1** was obtained in higher yields due to the extensive optimization previously performed. To increase the RCY of the other probes, similar studies might be required. Regarding pre-targeting performance *in vivo* , [^{18}F]**4** demonstrated superior tumor accumulation but also prolonged blood retention. Thus, [^{18}F]**2** showed the highest tumor-to-background ratios 3 h after injection. Based on these results, [^{18}F]**2** and [^{18}F]**4** appear to outperform their corresponding dicarboxylic acid derivatives ([^{18}F]**1** and [^{18}F]**3**, respectively), suggesting that a net charge of 0 might be ideal to achieve higher tumor accumulation and faster clearance. It is evident that various factors may influence target accumulation of pretargeted tetrazines, and further optimization of these factors is warranted for lead compounds [^{18}F]**4** and [^{18}F]**2** prior to clinical translation.

ASSOCIATED CONTENT

Supporting Information

The Supporting Information is available free of charge at https://pubs.acs.org/doi/10.1021/acs.molpharmaceut.4c01129.

Additional experimental methods, details, HPLC and radio-HPLC data, elaborated *in vivo* data, and NMR spectra (PDF)

AUTHOR INFORMATION

Corresponding Authors

Lars Hvass − *Cluster for Molecular Imaging, Department of Biomedical Sciences, University of Copenhagen, 2200 Copenhagen N, Denmark; Department of Clinical Physiology, Nuclear Medicine & PET, Rigshospitalet, 2100 Copenhagen, Denmark;* orcid.org/0000-0003-2048-2409; Email: lars.hvass@sund.ku.dk

Umberto M. Battisti − *Department of Drug Design and Pharmacology, Faculty of Health and Medical Sciences, University of Copenhagen, 2100 Copenhagen, Denmark;* orcid.org/0000-0002-1012-8644; Email: akjaer@sund.ku.dk

Matthias M. Herth − *Department of Clinical Physiology, Nuclear Medicine & PET, Rigshospitalet, 2100 Copenhagen, Denmark; Department of Drug Design and Pharmacology, Faculty of Health and Medical Sciences, University of Copenhagen, 2100 Copenhagen, Denmark;* orcid.org/0000-0002-7788-513X; Email: matthias.herth@sund.ku.dk

Andreas Kjaer − *Cluster for Molecular Imaging, Department of Biomedical Sciences, University of Copenhagen, 2200 Copenhagen N, Denmark; Department of Clinical Physiology, Nuclear Medicine & PET, Rigshospitalet, 2100 Copenhagen, Denmark;* orcid.org/0000-0002-2706-5547; Email: umberto.battisti@sund.ku.dk

Authors

Marius Müller − *Department of Clinical Physiology, Nuclear Medicine & PET, Rigshospitalet, 2100 Copenhagen, Denmark; Department of Drug Design and Pharmacology, Faculty of Health and Medical Sciences, University of Copenhagen, 2100 Copenhagen, Denmark;* orcid.org/0000-0003-1882-5919

Markus Staudt − *Department of Drug Design and Pharmacology, Faculty of Health and Medical Sciences, University of Copenhagen, 2100 Copenhagen, Denmark;* orcid.org/0000-0002-7712-1818

Rocio García-Vázquez − *Department of Clinical Physiology, Nuclear Medicine & PET, Rigshospitalet, 2100 Copenhagen, Denmark; Department of Drug Design and Pharmacology, Faculty of Health and Medical Sciences, University of Copenhagen, 2100 Copenhagen, Denmark*

Tobias K. Gustavsson − *Department of Drug Design and Pharmacology, Faculty of Health and Medical Sciences, University of Copenhagen, 2100 Copenhagen, Denmark*

Vladimir Shalgunov − *Department of Drug Design and Pharmacology, Faculty of Health and Medical Sciences, University of Copenhagen, 2100 Copenhagen, Denmark;* orcid.org/0000-0001-8956-1207

Jesper T. Jørgensen − *Cluster for Molecular Imaging, Department of Biomedical Sciences, University of Copenhagen, 2200 Copenhagen N, Denmark; Department of Clinical Physiology, Nuclear Medicine & PET, Rigshospitalet, 2100 Copenhagen, Denmark*

Complete contact information is available at: https://pubs.acs.org/10.1021/acs.molpharmaceut.4c01129

Author Contributions

[‖]L.H. and M.M. contributed equally

Notes

The authors declare no competing financial interest.

■ ACKNOWLEDGMENTS

This work was supported by Danmarks Frie Forskningsfond (1032-0017B), the Lundbeck Foundation (grant R-303-2018-3567), EU (Horizon 2020 Framework program, grants 670261 and 668532), Danish National Research Foundation, grant 126. A.K. is a Lundbeck Professor (grant R310:2019:167)

■ REFERENCES

(1) Stéen, E. J. L.; Edem, P. E.; Nørregaard, K.; Jørgensen, J. T.; Shalgunov, V.; Kjaer, A.; Herth, M. M. Pretargeting in nuclear imaging and radionuclide therapy: Improving efficacy of theranostics and nanomedicines. *Biomaterials* **2018**, *179*, 209.

(2) Altai, M.; Membreno, R.; Cook, B.; Tolmachev, V.; Zeglis, B. M. Pretargeted Imaging and Therapy. *J. Nucl. Med.* **2017**, *58*, 1553.

(3) Bauer, D.; Cornejo, M. A.; Hoang, T. T.; Lewis, J. S.; Zeglis, B. M. Click Chemistry and Radiochemistry: An Update. *Bioconjug Chem.* **2023**, *34*, 1925.

(4) Lopes van den Broek, S.; Shalgunov, V.; García Vázquez, R.; Beschorner, N.; Bidesi, N. S. R.; Nedergaard, M.; Knudsen, G. M.; Sehlin, D.; Syvänen, S.; Herth, M. M. Pretargeted Imaging beyond the Blood-Brain Barrier-Utopia or Feasible? *Pharmaceuticals* **2022**, *15*, 1191.

(5) Shalgunov, V.; Lopes van den Broek, S.; Vang Andersen, I.; García Vázquez, R.; Raval, N. R.; Palner, M.; Mori, Y.; Schäfer, G.; Herrmann, B.; Mikula, H.; et al. Pretargeted imaging beyond the blood−brain barrier. *RSC Med. Chem.* **2023**, *14*, 444.

(6) Shalgunov, V.; van den Broek, S. L.; Andersen, I. V.; Raval, N. R.; Schäfer, G.; Barz, M.; Herth, M. M.; Battisti, U. M. Evaluation of F-537-Tetrazine in a model for brain pretargeting imaging. Comparison to N-(3-[^{18}F] fluoro-5-(1,2,4,5-tetrazin-3-yl)benzyl)-propan-1-amine. *Nucl. Med. Biol.* **2024**, *128*−*129*, 108877.

(7) Cook, B. E.; Archbold, J.; Nasr, K.; Girmay, S.; Goldstein, S. I.; Li, P.; Dandapani, S.; Genung, N. E.; Tang, S.-P.; McClusky, S.; et al. Non-invasive Imaging of Antisense Oligonucleotides in the Brain via In Vivo Click Chemistry. *Mol. Imaging Biol.* **2022**, *24*, 940.

(8) Scinto, S. L.; Bilodeau, D. A.; Hincapie, R.; Lee, W.; Nguyen, S. S.; Xu, M.; am Ende, C. W.; Finn, M. G.; Lang, K.; Lin, Q.; Pezacki, J. P.; Prescher, J. A.; Robillard, M. S.; Fox, J. M. Bioorthogonal chemistry. *Nature Reviews Methods Primers* **2021**, *1*, 30.

(9) Bird, R. E.; Lemmel, S. A.; Yu, X.; Zhou, Q. A. Bioorthogonal Chemistry and Its Applications. *Bioconjug Chem.* **2021**, *32*, 2457.

(10) García-Vázquez, R.; Battisti, U. M.; Herth, M. M. Recent Advances in the Development of Tetrazine Ligation Tools for Pretargeted Nuclear Imaging. *Pharmaceuticals* **2022**, *15*, 685.

(11) Tomarchio, E. G.; Turnaturi, R.; Saccullo, E.; Patamia, V.; Floresta, G.; Zagni, C.; Rescifina, A. Tetrazine−trans-cyclooctene ligation: Unveiling the chemistry and applications within the human body. *Bioorg Chem.* **2024**, *150*, 107573.

(12) Adhikari, K.; Vanermen, M.; Da Silva, G.; Van den Wyngaert, T.; Augustyns, K.; Elvas, F. Trans-cyclooctene—a Swiss army knife for bioorthogonal chemistry: exploring the synthesis, reactivity, and applications in biomedical breakthroughs. *EJNMMI Radiopharm Chem.* **2024**, *9*, 47.

(13) Blackman, M. L.; Royzen, M.; Fox, J. M. Tetrazine Ligation: Fast Bioconjugation Based on Inverse-Electron-Demand Diels−Alder Reactivity. *J. Am. Chem. Soc.* **2008**, *130*, 13518.

(14) Ruivo, E.; Adhikari, K.; Elvas, F.; Fissers, J.; Vangestel, C.; Staelens, S.; Stroobants, S.; Van der Veken, P.; Wyffels, L.; Augustyns, K. Improved stability of a novel fluorine-18 labeled TCO analogue for pretargeted PET imaging. *Nucl. Med. Biol.* **2019**, *76*, 36.

(15) Adhikari, K.; Dewulf, J.; Vangestel, C.; Van der Veken, P.; Stroobants, S.; Elvas, F.; Augustyns, K. Characterization of Structurally Diverse ^{18}F-Labeled d-TCO Derivatives as a PET Probe for Bioorthogonal Pretargeted Imaging. *ACS Omega* **2023**, *8*, 38252.

(16) wyffels, L.; Thomae, D.; Waldron, A.-M.; Fissers, J.; Dedeurwaerdere, S.; Van der Veken, P.; Joossens, J.; Stroobants, S.; Augustyns, K.; Staelens, S. In vivo evaluation of ^{18}F-labeled TCO for pre-targeted PET imaging in the brain. *Nucl. Med. Biol.* **2014**, *41*, 513.

(17) Rossin, R.; Renart Verkerk, P.; van den Bosch, S. M.; Vulders, R. C. M.; Verel, I.; Lub, J.; Robillard, M. S. In Vivo Chemistry for Pretargeted Tumor Imaging in Live Mice. *Angew. Chem. Int. Ed.* **2010**, *49*, 3375.

(18) Lewis, M. R.; Wang, M.; Axworthy, D. B.; Theodore, L. J.; Mallet, R. W.; Fritzberg, A. R.; Welch, M. J.; Anderson, C. J. In Vivo Evaluation of Pretargeted ^{64}Cu for Tumor Imaging and Therapy. *J. Nucl. Med.* **2003**, *44*, 1284.

(19) Zeglis, B. M.; Sevak, K. K.; Reiner, T.; Mohindra, P.; Carlin, S. D.; Zanzonico, P.; Weissleder, R.; Lewis, J. S. A Pretargeted PET Imaging Strategy Based on Bioorthogonal Diels−Alder Click Chemistry. *J. Nucl. Med.* **2013**, *54*, 1389.

(20) Meyer, J.-P.; Kozlowski, P.; Jackson, J.; Cunanan, K. M.; Adumeau, P.; Dilling, T. R.; Zeglis, B. M.; Lewis, J. S. Exploring Structural Parameters for Pretargeting Radioligand Optimization. *J. Med. Chem.* **2017**, *60*, 8201.

(21) Denk, C.; Svatunek, D.; Mairinger, S.; Stanek, J.; Filip, T.; Matscheko, D.; Kuntner, C.; Wanek, T.; Mikula, H. Design, Synthesis, and Evaluation of a Low-Molecular-Weight ^{11}C-Labeled Tetrazine for Pretargeted PET Imaging Applying Bioorthogonal in Vivo Click Chemistry. *Bioconjug Chem.* **2016**, *27*, 1707.

(22) García-Vázquez, R.; Battisti, U. M.; Shalgunov, V.; Schäfer, G.; Barz, M.; Herth, M. M. [^{11}C]Carboxylated Tetrazines for Facile Labeling of Trans-Cyclooctene-Functionalized PeptoBrushes. *Macromol. Rapid Commun.* **2022**, *43*, 2100655.

(23) Albu, S. A.; Al-Karmi, S. A.; Vito, A.; Dzandzi, J. P. K.; Zlitni, A.; Beckford-Vera, D.; Blacker, M.; Janzen, N.; Patel, R. M.; Capretta, A.; et al. 125I-Tetrazines and Inverse-Electron-Demand Diels−Alder Chemistry: A Convenient Radioiodination Strategy for Biomolecule Labeling, Screening, and Biodistribution Studies. *Bioconjug Chem.* **2016**, *27*, 207.

(24) Radjani Bidesi, N. S.; Battisti, U. M.; Lopes van de Broek, S.; Shalgunov, V.; Dall, A.-M.; Bøggild Kristensen, J.; Sehlin, D.; Syvänen, S.; Moos Knudsen, G.; Herth, M. M. Development of the First Tritiated Tetrazine: Facilitating Tritiation of Proteins. *ChemBioChem.* **2022**, *23*, No. e202200539.

(25) Denk, C.; Wilkovitsch, M.; Aneheim, E.; Herth, M. M.; Jensen, H.; Lindegren, S.; Mikula, H. Multifunctional Clickable Reagents for Rapid Bioorthogonal Astatination and Radio-Crosslinking. *ChemPlusChem.* **2019**, *84*, 775.

(26) Muller, M.; Battisti, U. M.; Zabrocki, M.; Hansson, E.; Jensen, H.; Aneheim, E.; Lindegren, S.; Herth, M. ^{211}At-Astatination of Arenes Using Trimethylgermanyl Precursors. *ChemPlusChem.* **2024**, *89*, e202400254.

(27) Otaru, S.; Paulus, A.; Imlimthan, S.; Kuurne, I.; Virtanen, H.; Liljenbäck, H.; Tolvanen, T.; Auchynnikava, T.; Roivainen, A.; Helariutta, K.; et al. Development of [^{18}F]AmBF3 Tetrazine for Radiolabeling of Peptides: Preclinical Evaluation and PET Imaging of [^{18}F]AmBF3-PEG7-Tyr3-Octreotide in an AR42J. Pancreatic Carcinoma Model. *Bioconjug Chem.* **2022**, *33*, 1393.

(28) Auchynnikava, T.; Äärelä, A.; Liljenbäck, H.; Järvinen, J.; Andriana, P.; Kovacs, L.; Rautio, J.; Rajander, J.; Virta, P.; Roivainen, A.; et al. Tetrazine Glycoconjugate for Pretargeted Positron Emission

Tomography Imaging of trans-Cyclooctene-Functionalized Molecular Spherical Nucleic Acids. *ACS Omega* **2023**, *8*, 45326.
(29) Beaufrez, J.; Guillouet, S.; Seimbille, Y.; Perrio, C. Synthesis, Fluorine-18 Radiolabeling, and In Vivo PET Imaging of a Hydrophilic Fluorosulfotetrazine. *Pharmaceuticals* **2023**, *16*, 636.
(30) Yang, C.; Lu, K.; Li, J.; Wu, H.; Chen, W. Rapid Construction of ^{18}F-Triazolyl-tetrazines through the Click Reaction. *J. Org. Chem.* **2024**, *89*, 14673.
(31) Denk, C.; Svatunek, D.; Filip, T.; Wanek, T.; Lumpi, D.; Fröhlich, J.; Kuntner, C.; Mikula, H. Development of a ^{18}F-Labeled Tetrazine with Favorable Pharmacokinetics for Bioorthogonal PET Imaging. *Angew. Chem. Int. Ed.* **2014**, *53*, 9655.
(32) Schlein, E.; Rokka, J.; Odell, L. R.; van den Broek, S. L.; Herth, M. M.; Battisti, U. M.; Syvänen, S.; Sehlin, D.; Eriksson, J. Synthesis and evaluation of fluorine-18 labelled tetrazines as pre-targeting imaging agents for PET. *EJNMMI Radiopharm Chem.* **2024**, *9*, 21.
(33) Keinänen, O.; Li, X.-G.; Chenna, N. K.; Lumen, D.; Ott, J.; Molthoff, C. F. M.; Sarparanta, M.; Helariutta, K.; Vuorinen, T.; Windhorst, A. D.; et al. A New Highly Reactive and Low Lipophilicity Fluorine-18 Labeled Tetrazine Derivative for Pretargeted PET Imaging. *ACS Med. Chem. Lett.* **2016**, *7*, 62.
(34) Stéen, E. J. L.; Jørgensen, J. T.; Denk, C.; Battisti, U. M.; Nørregaard, K.; Edem, P. E.; Bratteby, K.; Shalgunov, V.; Wilkovitsch, M.; Svatunek, D.; et al. Lipophilicity and Click Reactivity Determine the Performance of Bioorthogonal Tetrazine Tools in Pretargeted In Vivo Chemistry. *ACS Pharmacol Transl Sci.* **2021**, *4*, 824.
(35) Battisti, U. M.; Bratteby, K.; Jørgensen, J. T.; Hvass, L.; Shalgunov, V.; Mikula, H.; Kjær, A.; Herth, M. M. Development of the First Aliphatic ^{18}F-Labeled Tetrazine Suitable for Pretargeted PET Imaging—Expanding the Bioorthogonal Tool Box. *J. Med. Chem.* **2021**, *64*, 15297.
(36) García-Vázquez, R.; Jørgensen, J. T.; Bratteby, K. E.; Shalgunov, V.; Hvass, L.; Herth, M. M.; Kjær, A.; Battisti, U. M. Development of ^{18}F-Labeled Bispyridyl Tetrazines for In Vivo Pretargeted PET Imaging. *Pharmaceuticals* **2022**, *15*, 245.
(37) Andersen, I. V.; García-Vázquez, R.; Battisti, U. M.; Herth, M. M. Optimization of Direct Aromatic ^{18}F-Labeling of Tetrazines. *Molecules* **2022**, *27* (13), 4022.
(38) Battisti, U. M.; Müller, M.; García-Vázquez, R.; Herth, M. M. Labeling of Highly Reactive Tetrazines using [^{18}F]SuFEx. *Synlett* **2024**, *35*, 2207.
(39) García-Vázquez, R.; Battisti, U. M.; Jørgensen, J. T.; Shalgunov, V.; Hvass, L.; Stares, D. L.; Petersen, I. N.; Crestey, F.; Löffler, A.; Svatunek, D.; et al. Direct Cu-mediated aromatic ^{18}F-labeling of highly reactive tetrazines for pretargeted bioorthogonal PET imaging. *Chem. Sci.* **2021**, *12*, 11668.
(40) Greenwood, H. E.; Nyitrai, Z.; Mocsai, G.; Hobor, S.; Witney, T. H. High-Throughput PET/CT Imaging Using a Multiple-Mouse Imaging System. *J. Nucl. Med.* **2020**, *61*, 292.
(41) Knight, J. C.; Mosley, M.; Uyeda, H. T.; Cong, M.; Fan, F.; Faulkner, S.; Cornelissen, B. In Vivo Pretargeted Imaging of HER2 and TAG-72 Expression Using the HaloTag Enzyme. *Mol. Pharmaceutics* **2017**, *14*, 2307.
(42) Martensson, L.; Nilsson, R.; Ohlsson, T.; Sjogren, H. O.; Strand, S. E.; Tennvall, J. Improved tumor targeting and decreased normal tissue accumulation through extracorporeal affinity adsorption in a two-step pretargeting strategy. *Clin. Cancer Res.* **2007**, *13*, 5572s.
(43) Rossin, R.; Lappchen, T.; van den Bosch, S. M.; Laforest, R.; Robillard, M. S. Diels-Alder reaction for tumor pretargeting: in vivo chemistry can boost tumor radiation dose compared with directly labeled antibody. *J. Nucl. Med.* **2013**, *54*, 1989.
(44) Lumen, D.; Vugts, D.; Chomet, M.; Imlimthan, S.; Sarparanta, M.; Vos, R.; Schreurs, M.; Verlaan, M.; Lang, P. A.; Hippeläinen, E.; et al. Pretargeted PET Imaging with a TCO-Conjugated Anti-CD44v6 Chimeric mAb U36 and [^{89}Zr]Zr-DFO-PEG5-Tz. *Bioconjug Chem.* **2022**, *33*, 956.

https://doi.org/10.1021/acs.molpharmaceut.4c01129
Mol. Pharmaceutics 2025, 22, 1911−1919